

Mechanotunable monatomic metal structures at graphene edges

Ning Wei^{1,2}, Cheng Chang^{1,2}, Hongwei Zhu^{2,3,*} and Zhiping Xu^{1,2,*}

¹Applied Mechanics Laboratory, Department of Engineering Mechanics, Tsinghua University, Beijing 100084, China

²Center for Nano and Micro Mechanics, Tsinghua University, Beijing 100084, China

³School of Materials Science and Engineering, Key Laboratory of Materials Processing Technology, Tsinghua University, Beijing 100084, China

*Authors to whom correspondence should be addressed.

Emails: xuzp@tsinghua.edu.cn (Z.X), hongweizhu@tsinghua.edu.cn (H. Z.)

Monatomic metal (e.g. silver) structures could form preferably at graphene edges. Their structural and electronic properties are explored here by performing density functional theory based first-principles calculations. The results show that cohesion between metal atoms and electronic coupling between metal atoms and graphene edges offer remarkable structural stability. Outstanding mechanical properties of graphene allow tunable properties of the metal monatomic structures by applying mechanical loads. Moreover, metal rings and helices can form at open ends of carbon nanotubes and edges of twisted graphene ribbons. These findings suggest the role of graphene edges as an efficient one-dimensional template for low-dimensional metal structures that are mechanotunable.

1. Introduction

Monatomic metal structures such as metal chains, rings and helices have attracted notable attention for many years due to their roles as model systems for low-dimensional material studies, as well as the potential in promising applications such as quantum electronics.¹⁻⁴ The one-dimensional (1D) nature of these structures is the origin of a number of distinctive behaviors that are absent in their two-dimensional (2D, mono- or multi-layers) and bulk counterparts.⁵ For example, the Fermi-liquid picture for electrons breaks down spectacularly in 1D metals by displaying collective excitations involving spin and charge.² On the other hand, electron-phonon interaction and Peierls distortion break lattice symmetry and thus modify the electronic structures of 1D materials.⁶ Monatomic metal structures can be synthesized by mechanical cleavage of metal nanowires, or metal adatoms assembly epitaxially on the substrate.^{5, 7} However, structures from these techniques either lack of considerable structural stability in ambient conditions,¹ or suffer from strongly electronic coupling with the substrate that substantially breaks their 1D nature.⁴ Alternative methods to fabricate stable and well-controlled monatomic metals are thus desired for the research and applications of such a novel structure.

Graphene is another monatomic material that extends in two-dimension, featuring outstanding structural, mechanical, thermal stabilities and tunable electronic structures.⁸⁻¹⁰ There are also emerging interests in using graphene as templates in preparation of low-dimensional materials and structures.¹¹ Their tailored nanostructures such as nanoribbons and island offer a new dimension for this concept with their open edges for adhesive attachment and self-organization.¹²⁻¹⁴ In a recent experimental work, we reported in-situ synthesis of graphene-metal hybrids where silver nanoplates were obtained through the template effect of graphene.¹⁵ The results indicate that defected sites or edges of graphene are more preferable for metal binding.¹⁵ This observation gave us a hint of using the edge-template for low-dimensional metal structures, which will be addressed in this work. We performed first-principles calculations to explore the

structures and properties of several monatomic forms of metal, using Ag as an example, and analyzed their mechanical and electronic coupling. The results identify an efficient template function of graphene edges and lay the ground for future exploration on low-dimensional materials.

2. Methods

In this work, plane-wave-basis-set-based density functional theory (DFT) was employed for the first-principles calculations. We used Quantum-Espresso code for our DFT calculations.¹⁶ Both local density approximation (LDA), generalized gradient approximation (GGA) for the exchange-correlation energy and ultrasoft pseudopotentials for the ion-electron interactions were imposed.¹⁷ In our following discussion, GGA was used if not specified. Energy cut-offs of 37 and 370 Rydberg were set for the plane-wave basis set and charge density grid respectively. These settings were verified to achieve a total energy convergence below 1 meV per atom. The atomic structures were relaxed using the conjugated gradient algorithm, with converged force on atoms below 0.01 eVÅ⁻¹. In variable-cell relaxation for the periodic direction along graphene edge, the residue stress was controlled below 0.01 GPa. A Monkhorst-Pack grid with 12 k -points was used along the periodic direction for Brillouin zone integration, which was qualified to satisfy the energy convergence criterion of 1 meV.

3. Results and Discussion

3.1 Atomic structures and binding energies

To explore the mechanism of metal-graphene hybridization, we assigned silver atoms along both zigzag and armchair graphene edges of a graphene nanoribbon (GNR) and optimized their geometries under a stress-free condition along the ribbon. The equilibrated structure for the 1D isolated Ag monatomic structure features a zigzag pattern,³ and the interatomic distance is calculated in this work to be $a_{\text{Ag}} = 2.67 \text{ \AA}$, and the lattice constants for graphene along zigzag and armchair directions are $a_Z = 2.46 \text{ \AA}$

and $a_A = 4.26 \text{ \AA}$ respectively. We placed metal atoms with a maximum line density along the edge, corresponding to a lattice constant for the Ag chain $a_{Ag} = a_Z$ or a_A . The stabilities of metal binding were assessed by comparison with different binding sites at the edges (e.g. tips, valleys), as well as adatom positions on top of the hexagonal lattice of graphene (see annotations in **Figure 1**). To quantify the relative stabilities, a binding energy E_b was calculated by comparing total energy of the hybrid E_{G+nM} , the pristine GNR E_G and the isolated metal atom E_M , i.e. $E_b = (E_G + nE_M - E_{G+nM})/n$, where n is the number of metal atoms bound to graphene. Spin-nonpolarized DFT calculation results for both zigzag graphene nanoribbons (ZGNRs) with $w = 8$ and armchair graphene nanoribbons (AGNRs) with $w = 12, 13$, and 14 are summarized in **Figure 1**, which indicate distinctly that metal atoms prefer the valley sites at the GNR edges. Here the width w is defined as the number carbon chains along the width direction, following the convention used in Ref. 18. In these calculations, single unit cell of the graphene was used and thus the Ag atoms take a linear chain configuration. The calculated binding energies for adatoms on the hexagonal lattice are lower when binding sites are close to edges. After binding metallic atoms at its edge, the graphene ribbon has no out-of-plane distortion due to its well-preserved aromatic nature. The carbon-carbon bond length at the edge changes slightly (e.g. from 0.138 to 0.141 nm for ZGNR), resulting from charge transfer between Ag and C atoms and additional interaction between Ag atoms. In the hybrid the interatomic distance between metal atoms are defined by the lattice constant of graphene. It should also be noted that the energy difference between metal binding at sites 1, 2 and 3 (as annotated in **Figure 1**) for the Ag-ZGNR hybrid are $\sim 0.1 \text{ eV}$ from both LDA and GGA calculations. This amplitude of energy difference is not significantly high compared to thermal energy ($k_B T \sim 26 \text{ meV}$ at ambient conditions) and thus cannot be distinguished at elevated ambient temperature. Thicker metal decoration, such as clusters or nanowires, may form due to the presence of thermal fluctuation, perturbation from substrates, at a high density of metal atoms near the edges.

The formation of metal-graphene hybrids can be discussed along two reaction paths, noted as paths **a** and **b** in this work. Each path includes a two-step process. Along path **a**, metal atoms first assemble into an isolated one-dimensional metal chain. Then the chain attaches to the graphene edge and the hybrid forms. While along path **b**, metal atoms attach to the graphene edges one by one first, and then form a continuous metal chain at the edge. In path **b**, we neglected the effect of neighboring metal atoms when calculate the binding energy for a metal atom to the edge, by using a four-period supercell along the ribbon direction. The formation energies can thus be defined through two terms for each path, i.e. $E_{a1} = E_{MC}/N - E_M$, $E_{a2} = E_{MCG}/N - (E_{MC}/N + E_G/N)$, $E_{b1} = E_{MG} - (E_M + E_G/N)$, $E_{b2} = E_{MCG}/N - E_{MG}$, where N is the number of unit cells for the metal-graphene hybrid, and subscripts M, MC, MG, MCG stand for the metal atom, metal chain, single metal atom attachment to the edge, and the hybrid consisting of a metal chain attached to the graphene edge. The results for Ag-ZGNR with $w = 8$ are $E_{a1} = -1.21$ eV, $E_{a2} = -1.66$ eV; $E_{b1} = -3.48$ eV, $E_{b2} = 0.41$ eV, which suggest that along path **a**, two steps are both energetically favorable, while along path **b**, an energy penalty is required to densify the monatomic structure of metals along the edge and thus discrete clusters or structures with larger lattice constant a_{Ag} could form.

More specifically for path **b**, where the metal monatomic structures grow on the edge, we consider the initial steps of metal binding. After an Ag atom is attached to the zigzag edge of graphene, the second atom could attach at the nearest-neighbor or the second nearest-neighbor sites. These two sites offer binding energies of 3.32 and 3.41 eV respectively for the second Ag atom, lower than the value for the first attachment (3.48 eV). Moreover, the nearest binding requires 0.1 eV more energy due to the repulsive force between Ag atoms. Thus the growth of Ag monatomic structures at graphene edges could start by forming low-density patterns and then being refined. The third atom could thus attach to the position along the edge, or on top of the pre-existing Ag dimer and form a trimer. Our calculations show that the edge position is 0.77 eV more preferred, and the

energy barrier for the metal atom to diffuse from the trimer position to the edge is calculated to be ~ 0.5 eV.

Earlier studies on Ag monatomic chains indicated that zigzag configuration forms in isolated Ag chains or Ag chains bound at zigzag graphene edges.^{3,19} In order to include the alternation in positions of metal atoms along graphene edge, a double-period supercell for ZGNR was used. Random displacement perturbation was added to the Ag atoms in all three directions with amplitude of 0.1 \AA , to break the mirror symmetry along the graphene edge. From the calculation results, we found that there are two types of termination of Ag atoms aligned to graphene edges, i.e. at the tip or valley positions of the edge, both featuring a zigzag pattern with respect to the graphene basal plane. As the equilibrium Ag-Ag distance in a metal chain (2.67 \AA) is larger than the length of a ZGNR unit cell (2.46 \AA), the metal chain thus prefers zigzag structures after it is bounded to the graphene edge, and the valley configuration illustrated in **Figure 1e** is more favorable in binding energy (by 0.05 eV compared to the tip configuration). This can also be seen from structural information of the Ag-ZGNR hybrid summarized in **Table 1**, which shows an Ag-Ag distance of 2.67 \AA in the zigzag chain, and Ag-C distance of 2.35 \AA . The binding energies E_b , i.e. 2.82 and 2.87 eV for the tip and valley configurations, are more than two-fold higher than E_b for Ag in an isolated chain with the same configuration. These results also suggest that the interaction between Ag atoms makes a significant contribution to the structural stability of Ag-ZGNR hybrid.

For AGNRs, as the interatomic distance between neighboring Ag atoms (4.26 \AA) is larger than the value in the Ag chain (2.67 \AA), no out-of-plane displacement of the Ag atoms was observed due to the weakened interaction between Ag atoms along the graphene edges. The binding of metal atoms to both ZGNR and AGNR edges features apparent density dependence due to the interatomic coupling between Ag atoms. Our first-principles calculations show that an isolated zigzag Ag chain is stable at the interatomic distance $d = 2.67 \text{ \AA}$. However, a structural transition to the linear

configuration occurs with $d = 2.78 \text{ \AA}$ after it is elongated, and the chain eventually fails at $d = 3.0 \text{ \AA}$. These results further confirm our observation that the interatomic interaction between Ag is repulsive for Ag-ZGNR at $a_{\text{Ag}} = a_z$, and almost zero for Ag-AGNR $a_{\text{Ag}} = a_A$. One would thus expect for Ag-ZGNR with $a_{\text{Ag}} = 2a_z$, the Ag-Ag interaction will be negligible and a linear configuration will be more favorable, at a reduced density. This was verified by our DFT calculations.

3.2 Electronic coupling

We now turn to discuss the electronic coupling between metal atoms and graphene edges. Bader atomic charge analysis suggests that $0.25e$ charge is transferred from Ag atoms to carbon atoms at valley sites along the edge of ZGNR for $w = 8$. While for AGNRs, the charge transfer is $0.34e$ for $w = 12, 13, 14$. The results also indicate that for both AGNRs and ZGNRs, the metal atoms binding favors valley sites at graphene edges where carbon atoms have two dangling bonds. In contrast, the charge transfer from Ag atoms on top of graphene is much lower, i.e. $0.029e$ and $0.022e$ for ZGNR and AGNR (at sites 5 and 6 in **Figure 1a** and **1b**). To further characterize the bonding nature between metal and graphene, distribution of the electron localization function (ELF)²⁰ was calculated. ELF is a localized function of the ground-state electron density and wavefunction obtained from first-principles calculations. The value of ELF ranges from 0 to 1, where 1 corresponds to the perfect localization as in covalent bonds, and 0.5 corresponds to the electron-gas-like pair probability as in metallic bonds. The results in **Figure 2** thus suggest an ionic nature of Ag-GNR interaction.

These results, in combination with previous discussion on the binding energies, clearly suggest that in addition to the adhesion of metal atoms at the edge, the electrostatic cohesion between metal atoms is also a key driving force to stabilize the hybrid structures, as template at graphene edges. To explore the perturbation of metal binding to the electronic structures of both metal and graphene, we analyzed band structures and

density of states (DOS) calculated from spin-polarized DFT calculations. We considered the hybrid structures with metal atoms bound to both sides of the ZGNR. Antiferromagnetic (AFM), ferromagnetic (FM) and paramagnetic (PM) states were identified. The difference in energy is 51.9 meV per unit cell lower for both AFM and FM than PM ordering, and the difference between AFM and FM states is below 1 meV. Calculated band structures shown in **Figure 3** suggest that the electronic coupling between Ag atoms and ZGNR is weak. Charge transfer upshifts bands for electrons in Ag and downshifts those for electrons in graphene. As a result, Ag band will not cross the Fermi energy, in contrast to the monatomic Ag chain. Additionally, the localized states attributed to the dangling bonds at graphene edges were removed by Ag-termination. Thus the electronic structure of Ag monatomic structures formed remains to be relatively intact, and the graphene edges is doped in *n*-type.

3.3 Strain effects

One of the signature characteristics of graphene is exceptional mechanical stability, which enables strain engineering under tensile strain up to $\sim 20\%$. Thus by straining the GNRs we could tune the monatomic metal structures accordingly, which is not allowed in monatomic metal wires formed on the metal substrates.¹⁻⁴ To illustrate the structural evolution of the Ag-ZGNR hybrid (with Ag in the valley position) as a function of axial strain along the graphene ribbon, we performed tensile tests and monitored the variation in the atomic structure. As shown in **Figure 4a**, the out-of-plane displacement of Ag atoms relative to the graphene basal plane surface decreases with strain and becomes zero at 11% strain. Changes in the Ag-Ag and Ag-C distances depicted in **Figure 4b** shows that before the Ag monatomic structure is flattened to the graphene basal plane, the Ag-Ag distance remains the same, and the structure evolves only by changing the angle between them. In contrast, the graphene is strained affinely and thus defines the mechanical response of the hybrid before it breaks down by fracture of the hexagonal lattice. Accordingly the mechanical properties of the hybrid (stiffness, strength, strain to

failure, etc.) are comparable to graphene. Our calculations verified this by demonstrating the strain to failure as 24%, the same as the value for graphene and higher than the value 21.74% defined by the Ag chain. The fracture eventually nucleates by breaking C-C bonds in the graphene lattice. Thus the monatomic Ag structure formed could be tuned from a zigzag configuration to a linear chain with interatomic distance ranging from 2.67 to 3.06 Å, beyond which the hybrid structure fails.

3.4 Metal rings and other monatomic structures

With the results obtained above for (straight, zigzag) monatomic metal structures formed at graphene edges, more low-dimensional structures could be envisioned. For example, two illustrative examples were explored here by first-principles calculations, including metal rings formed at ends of carbon nanotubes, and metal helices formed at edges of twisted GNRs.^{21,22} The results show that both these structures are comparably stable with Ag atoms aligned at graphene edges. The structures and electronic density of states (DOS) for Ag-CNT hybrid are summarized in **Table 2** and **Figure 5**, which is consistent with the picture of weak coupling between Ag and CNT ends. Moreover, an alternative pattern of radial displacement (type II) is preferred for small-diameter CNTs (6, 6) and (8, 8), while for (10, 10) CNT with a larger diameter, configuration (type I) with all Ag atoms residing outside of the CNT is preferred. This concept of templating low-dimensional metal structures using graphene edges could be further extended, for example, in forming thin nanowires of metals at the edges of bilayer or multilayer graphene sheets that are staggered, or mono- and multilayers on the basal plane of graphene sheets.^{9,23} It is worth noting that the binding energy of Ag at ZGNR edges is 2.82 eV, that is even higher than Ag in the close-packing 2D triangular lattice (1.92 eV) and 3D face-centered-cubic (FCC) lattice (2.62 eV). Thus these metal nanostructures formed at graphene edges features significant structural stabilities, as demonstrated in our previous experiments.¹⁵

Although main discussion in this paper is based on Ag hybrid, we also explored binding of Au and Ni atoms at graphene edges that share the common feature of preferred edge binding as we identified for Ag. These hybrids are interesting as Au nanowire assembled at graphene edges is expected to be more stable than Ag due to its resistance to oxidation, while the presence of *d*-electrons in Ni implies interesting magnetic behaviors. Our additional calculations show that the formation of monatomic Au and Ni structures at graphene edges are also energy favorable.

The bare edges of graphene are not stable in ambient condition and could be terminated by chemical groups such as hydrogen. We probed the effect of H-termination by performing DFT calculations with metal atoms placed at the tip and valley positions from the hydrogen atoms. The results summarized in **Table 1** suggest that although the coupling between Ag atoms and graphene edge is weakened, the binding energy 1.24 eV is still significant enough to provide considerable stability at ambient conditions. The value is also close to the binding energy in the isolated Ag chain with the same configuration (1.21 eV). This result thus further validates our conclusion that as the cohesion between metal atoms is one of the major driving forces for the assembly of metal monatomic structures along graphene edges.

4. Conclusion

To conclude, our first-principles calculations have revealed that metallic decoration of graphene nanostructures is favored at their edges, the stability is attributed to cohesion between metal atoms, as well as metal-graphene interaction. The weak electrostatic coupling between metal atoms and graphene, and the outstanding structural stabilities and mechanical properties of graphene enable a robust templating approach with strain tunability, offering opportunities in low-dimensional material design and applications.

Acknowledgments

This work was supported by the National Natural Science Foundation of China through

Grant 11222217, 11002079, 51372133, Tsinghua University Initiative Scientific Research Program 2011Z02174, 2012Z02102, and the Tsinghua National Laboratory for Information Science and Technology of China.

TABLES, FIGURES AND FIGURE CAPTIONS

Table 1 Structure and energy information for the metal-ZGNR hybrids, including metal-metal (d_{M-M}) and metal-carbon (d_{M-C}) distances, the binding energies E_b for Ag attached to graphene edges, and binding energies E_{chain} of Ag in a monatomic chain with the same configuration as in the Ag-ZGNR hybrid.

structure	binding site	d_{M-M} (Å)	d_{M-C} (Å)	E_b (eV)	E_{chain} (eV)
Ag-ZGNR	tip	2.74	2.15	2.82	1.20
	valley	2.67	2.35	2.87	1.21
Ag-H-ZGNR	tip	2.67	4.26	1.24	1.21
	valley	2.67	4.54	1.24	1.21

Table 2 Structure and energy information for the Ag-CNT hybrid. Atomic structures of type I and II configurations are defined in **Figure 5**, where Ag atoms have the same or alternative radial distance from the carbon atoms in CNT. For type II, two different metal-carbon distances are both listed.

structure	type	d_{M-M} (Å)	d_{M-C} (Å)	E_b (eV)	E_{chain} (eV)
Ag-(6,6) CNT	Type I	2.65	2.39	2.64	1.18
	Type II	2.70	2.28/2.54	2.74	1.40
Ag-(8,8) CNT	Type I	2.65	2.37	2.71	1.11
	Type II	2.75	2.35/2.42	2.88	1.44
Ag-(10,10) CNT	Type I	2.65	2.37	2.77	1.17
	Type II	2.68	2.32/2.46	2.72	1.28

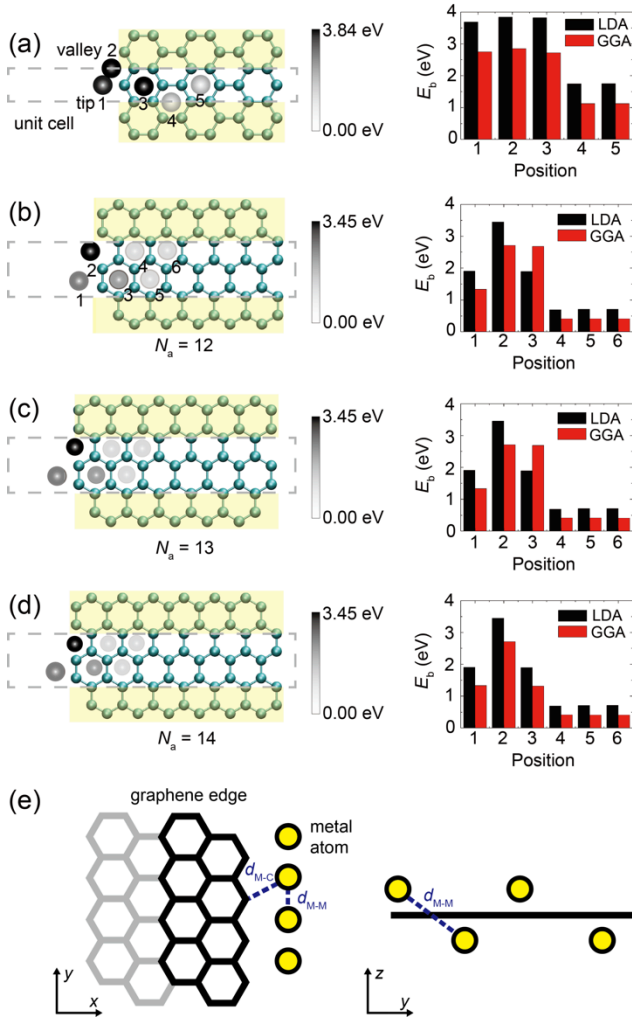


FIG. 1. Atomic structures and binding energies of metal atoms bound to graphene edges as a linear chain. (a-d) Binding sites of Ag atoms at ZGNR and AGNR edges, and their relative binding energies dictated by the gray level. (e) Zigzag metal monatomic structures formed at the valley sites of ZGNR edges. d_{M-C} and d_{M-M} are the metal-carbon and metal-metal distances in the hybrid mentioned in the text.

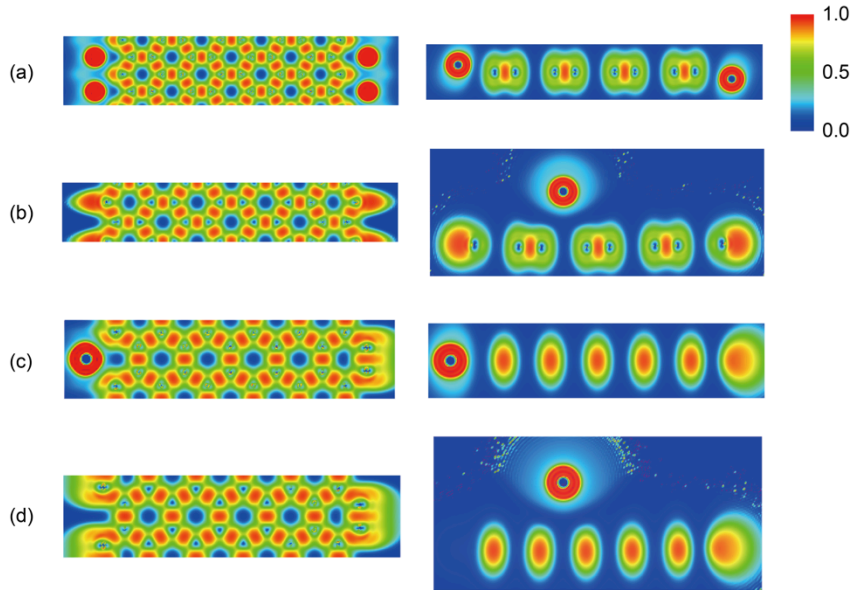


FIG. 2. Electron localized function distribution of (a, b) Ag-ZGNR and (c, d) Ag-AGNRs hybrids, with Ag atoms bound to the valley site at graphene edges (a, c) and on top of graphene (b, d). Both top view (left) and side view (right) are plotted.

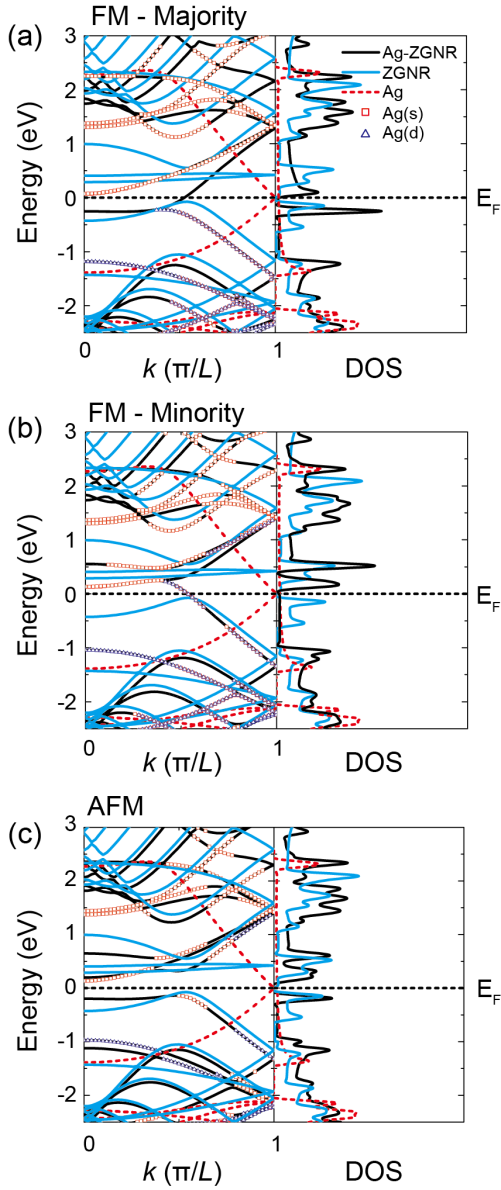


FIG. 3. Energy band structures (left) and density of state (DOS, right) for the Ag-ZGNR hybrid, zigzag Ag-chain and bare ZGNR, respectively. The projections on s - and d -orbitals of Ag atoms in the Ag-ZGNR are plotted using squares and triangles. (a) and (b) are for major and minor spin components in the FM state and (c) is for the AFM state.

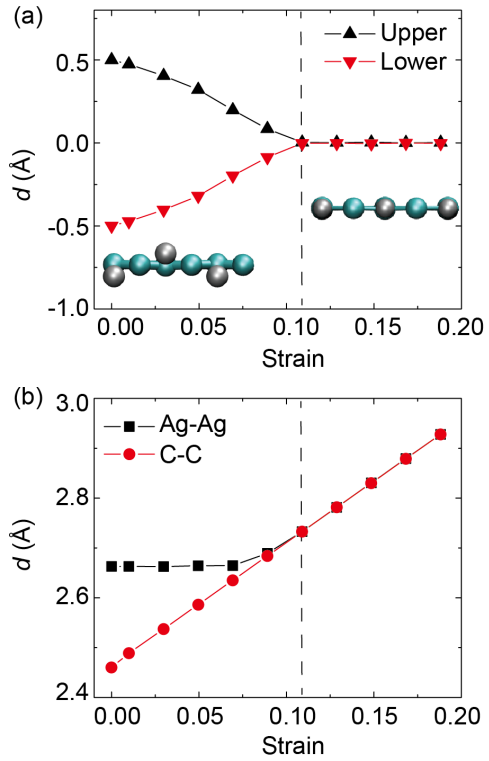


FIG. 4. (a) Out-of-plane displacement of Ag atoms measured a function of tensile strain on the double-period zigzag Ag-ZGNR hybrid with Ag at the valley position. (b) Distance between Ag-Ag atoms and C-C atoms at graphene edges, which becomes synchronized at 11% strain.

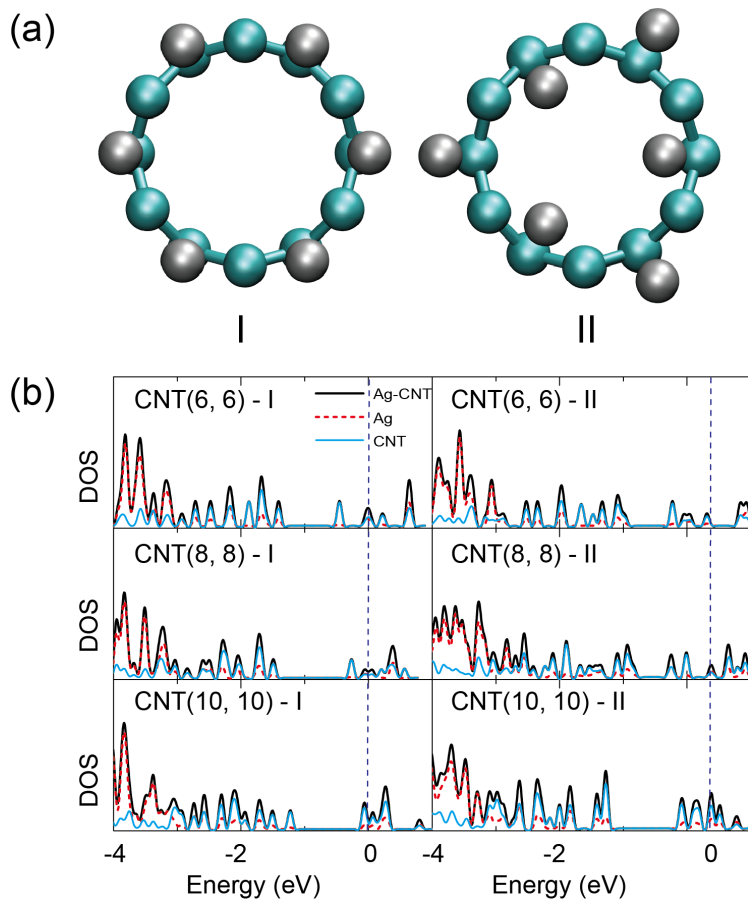


FIG. 5. Atomic structures (a) and DOS (b) for the Ag-CNT hybrids. In type I and II configurations, the Ag atoms have the same and alternative radial displacement with respect to carbon atoms in the CNT. The relative stabilities and geometry are summarized in **Table 2**.

REFERENCES

1. H. Ohnishi, Y. Kondo and K. Takayanagi, *Nature*, 1998, 395, 780-783.
2. P. Segovia, D. Purdie, M. Hengsberger and Y. Baer, *Nature*, 1999, 402, 504-507.
3. M. Springborg and Y. Dong, *Metallic Chains/Chains of Metals*, Elsevier, Amsterdam and Oxford, 2007.
4. P. A. Ignatiev, N. N. Negulyaev, L. Niebergall, H. Hashemi, W. Hergert and V. S. Stepanyuk, *Physica Status Solidi (b)*, 2010, 247, 2537-2549.
5. P. Gambardella, A. Dallmeyer, K. Maiti, M. C. Malagoli, W. Eberhardt, K. Kern and C. Carbone, *Nature*, 2002, 416, 301-304.
6. A. I. Yanson, G. R. Bollinger, H. E. van den Brom, N. Agrait and J. M. van Ruitenbeek, *Nature*, 1998, 395, 783-785.
7. P. Gambardella, *Journal of Physics: Condensed Matter*, 2003, 15, S2533.
8. T. J. Booth, P. Blake, R. R. Nair, D. Jiang, E. W. Hill, U. Bangert, A. Bleloch, M. Gass, K. S. Novoselov, M. I. Katsnelson and A. K. Geim, *Nano Letters*, 2008, 8, 2442-2446.
9. C. O. Girit, J. C. Meyer, R. Erni, M. D. Rossell, C. Kisielowski, L. Yang, C.-H. Park, M. F. Crommie, M. L. Cohen, S. G. Louie and A. Zettl, *Science*, 2009, 323, 1705-1708.
10. Z. Xu and K. Xue, *Nanotechnology*, 2010, 21, 045704.
11. H. Wang, J. T. Robinson, G. Diankov and H. Dai, *Journal of the American Chemical Society*, 2010, 132, 3270-3271.
12. Z. Xu, Q.-S. Zheng and G. Chen, *Applied Physics Letters*, 2007, 90, 223115-223113.
13. L. Ci, Z. Xu, L. Wang, W. Gao, F. Ding, K. Kelly, B. Yakobson and P. Ajayan, *Nano Research*, 2008, 1, 116-122.
14. Z. Xu and M. J. Buehler, *Nanotechnology*, 2009, 20, 375704.
15. Z. Li, P. Zhang, K. Wang, Z. Xu, J. Wei, L. Fan, D. Wu and H. Zhu, *Journal of*

- Materials Chemistry*, 2011, 21, 13241.
16. P. Giannozzi, S. Baroni, N. Bonini, M. Calandra, R. Car, C. Carlo, C. Davide, L. C. Guido, C. Matteo, D. Ismaila, C. Andrea Dal, G. Stefano de, F. Stefano, F. Guido, G. Ralph, G. Uwe, G. Christos, K. Anton, L. Michele, M.-S. Layla, M. Nicola, M. Francesco, M. Riccardo, P. Stefano, P. Alfredo, P. Lorenzo, S. Carlo, S. Sandro, S. Gabriele, P. S. Ari, A. Smogunov, P. Umari and R. M. Wentzcovitch, *Journal of Physics: Condensed Matter*, 2009, 21, 395502-395519.
 17. T. Filleter and H. D. Espinosa, *Carbon*, 2013, 56, 1-11.
 18. Y. W. Son, M. L. Cohen and S. G. Louie, *Physical Review Letters*, 2006, 97, 216803.
 19. Y. Wang, C. Cao and H.-P. Cheng, *Physical Review B*, 2010, 82, 205429.
 20. B. Silvi and A. Savin, *Nature*, 1994, 371, 683-686.
 21. K. Bets and B. Yakobson, *Nano Research*, 2009, 2, 161-166.
 22. V. B. Shenoy, C. D. Reddy, A. Ramasubramaniam and Y. W. Zhang, *Physical Review Letters*, 2008, 101, 245501.
 23. X. Jia, M. Hofmann, V. Meunier, B. G. Sumpter, J. Campos-Delgado, J. M. Romo-Herrera, H. Son, Y.-P. Hsieh, A. Reina, J. Kong, M. Terrones and M. S. Dresselhaus, *Science*, 2009, 323, 1701-1705.